

Scalarized Kerr-Newman Black Holes

Guangzhou Guo^{a,b,*}, Peng Wang^{a,†}, Houwen Wu^{a,c,‡} and Haitang Yang^{a,§}

^a*Center for Theoretical Physics, College of Physics,
Sichuan University, Chengdu, 610064, China*

^b*Department of Physics, Southern University of Science and Technology, Shenzhen, 518055, China and*

^c*Department of Applied Mathematics and Theoretical Physics,
University of Cambridge, Wilberforce Road, Cambridge, CB3 0WA, UK*

In this paper, we construct scalarized rotating black holes within the framework of Einstein-Maxwell-scalar models. These models incorporate non-minimal couplings that can induce tachyonic instabilities, leading to the spontaneous scalarization of Kerr-Newman (KN) black holes. By exploring the domain of existence, we observe that the presence of scalarized KN black holes is suppressed by the black hole spin, with a maximum spin threshold beyond which scalarized solutions cease to exist. Intriguingly, we find that in specific parameter regimes, scalarized KN black holes can exhibit the presence of two unstable and one stable light rings on the equatorial plane, manifesting in both prograde and retrograde directions.

arXiv:2307.12210v1 [gr-qc] 23 Jul 2023

* guangzhouguo@outlook.com

† pengw@scu.edu.cn

‡ hw598@damtp.cam.ac.uk

§ hyanga@scu.edu.cn

CONTENTS

I. Introduction	2
II. Einstein-Maxwell-scalar Model	4
A. Tachyonic Instability	5
B. Rotating Black Hole Solution	6
C. Light Ring	7
D. Numerical Scheme	8
III. Numerical Results	10
A. Domain of Existence	10
B. Light Ring Structure	11
IV. Conclusions	15
Acknowledgments	15
References	16

I. INTRODUCTION

In the past decade, the groundbreaking detections of gravitational waves from binary black hole mergers by LIGO and Virgo have opened up new avenues for testing general relativity in the strong field regime [1]. During the ringdown phase of a black hole merger, the emitted gravitational waves can be described by a superposition of quasinormal modes [2]. Extracting these quasinormal modes from the observed gravitational wave signals allows us to determine the properties of the remnant black hole, e.g., its mass, charge, and angular momentum, thus providing a promising tool to test the validity of the Kerr hypothesis [3, 4]. Furthermore, a significant breakthrough in the field of black hole observation was achieved with the recent release of images of the supermassive black holes M87* and Sgr A* by the Event Horizon Telescope (EHT) collaboration [5–16]. While the detections of gravitational waves and the observed black hole images align well with the predictions of Kerr black holes, it is worth noting that the limitations in observational resolution leave room for exploration of alternative theories and black hole mimics.

The no-hair theorem asserts that black holes are characterized exclusively by their mass, electric charge and angular momentum [17–19]. However, various models have been formulated that

give rise to hairy black holes endowed with additional degrees of freedom, thereby serving as counterexamples to the no-hair theorem [20–26]. One prominent counterexample is spontaneous scalarization, which typically occurs in models featuring non-minimal couplings between scalar fields and other fields. These coupling terms serve as sources that destabilize scalar-free black hole solutions and give rise to the formation of scalarized hairy black holes.

Initially explored in the context of scalar-tensor models for neutron stars, spontaneous scalarization was found when scalar fields are coupled to the Ricci curvature [27]. It was demonstrated that a coexistence region exists where scalar-free and scalarized neutron star solutions compete energetically, with the scalarized solutions often exhibiting a preference. Subsequently, it was discovered that spontaneous scalarization can also manifest in black hole spacetime in scalar-tensor models, provided that black holes are coupled to non-linear electrodynamics [28, 29] or surrounded by non-conformally invariant matter [30, 31]. More recently, the phenomenon of spontaneous scalarization has been investigated in extended Scalar-Tensor-Gauss-Bonnet (eSTGB) gravity [32–38]. In eSTGB models, the scalar field is non-minimally coupled to the Gauss-Bonnet curvature correction in the gravitational sector, which can induce the formation of spinning scalarized black holes [36, 37]. However, the presence of non-linear curvature terms in the eSTGB models brings numerical challenges in solving the evolution equations.

To gain a deeper understanding of the dynamical evolution leading to the formation of scalarized black holes, a technically simpler class of models called Einstein-Maxwell-scalar (EMS) models has been proposed [39]. These models incorporate non-minimal couplings between the scalar and Maxwell fields, which introduce tachyonic instabilities capable of triggering spontaneous scalarization. In [39], fully non-linear numerical simulations in spherical symmetry demonstrated the evolution of Reissner-Nordström (RN) black holes into scalarized RN black holes. Subsequent investigations of the EMS models have yielded a wealth of research findings, e.g., different non-minimal coupling functions [40–42], massive and self-interacting scalar fields [43, 44], horizonless reflecting stars [45], stability analysis of scalarized black holes [46–50], higher dimensional scalar-tensor models [51], quasinormal modes of scalarized black holes [52, 53], two U(1) fields [54], quasitopological electromagnetism [55], topology and spacetime structure influences [56], scalarized black hole solutions in the dS/AdS spacetime [57–61], and dynamical scalarization and descalarization [62–64].

Remarkably, scalarized RN black holes have been discovered to exhibit the presence of multiple photon spheres outside the event horizon in specific parameter regimes [65]. Subsequent investigations have focused on the optical appearances of various phenomena in the background of

scalarized RN black holes, e.g., accretion disks [65, 66], luminous celestial spheres [67] and infalling stars [68]. These studies have revealed that the existence of an additional photon sphere significantly increases the flux of observed accretion disk images, generates triple higher-order images of a luminous celestial sphere, and gives rise to an additional cascade of flashes from an infalling star. Furthermore, the presence of multiple photon spheres in a spacetime also suggests the existence of long-lived modes that may render the spacetime unstable [69–73]. Specifically, it has been shown that the existence of multiple photon spheres outside the event horizon can induce superradiance instabilities for charged scalar perturbations [74]. For a more detailed analysis of black holes with multiple photon spheres, we refer readers to the work [75].

Recently, it has been reported that tachyonic instabilities around Kerr-Newman (KN) black holes can lead to unstable scalar perturbations in the EMS model, indicating the existence of scalarized rotating black holes [76]. The aim of this paper is twofold: first, to numerically construct scalarized rotating black hole solutions in the EMS model; and second, to investigate whether scalarized rotating black holes possess multiple light rings. The rest of the paper is organized as follows. In Section II, we introduce the construction of scalarized KN black holes in the EMS model and discuss light rings on the equatorial plane. Subsequently, we present the numerical results for the scalarized black hole solutions and their light ring structure in Section III. We conclude our main results and provide discussions in Section IV. We set $G = c = 4\pi\epsilon_0 = 1$ throughout this paper.

II. EINSTEIN-MAXWELL-SCALAR MODEL

In the EMS model, where a scalar field is non-minimally coupled to electromagnetism, the background spacetime can become destabilized through a tachyonic instability, leading to the phenomenon of spontaneous scalarization in black holes. The corresponding action is described as

$$S = \frac{1}{16\pi} \int d^4x \sqrt{-g} [R - 2\partial_\mu\phi\partial^\mu\phi - f(\phi)F^{\mu\nu}F_{\mu\nu}], \quad (1)$$

where ϕ is the scalar field, $F_{\mu\nu} = \partial_\mu A_\nu - \partial_\nu A_\mu$ denotes the electromagnetic field strength tensor, and A_μ represents the electromagnetic field. It is important to note that to trigger spontaneous scalarization, the coupling function $f(\phi)$ between ϕ and A_μ should satisfy $f(0) = 1$ and $f'(0) \equiv df(\phi)/d\phi|_{\phi=0} = 0$ [39, 40]. In this paper, we focus on the specific exponential coupling function $f(\phi) = e^{\alpha\phi^2}$ with $\alpha > 0$. In this section, we present the numerical construction of scalarized KN black holes in the EMS model and investigate null circular geodesics (i.e., light rings) within these

scalarized KN black holes.

A. Tachyonic Instability

In the scalar-free background, represented by KN black holes, the scalar perturbation $\delta\phi$ is governed by the equation

$$(\square - \mu_{\text{eff}}^2) \delta\phi = 0, \quad (2)$$

where $\mu_{\text{eff}}^2 = \alpha F^{\mu\nu} F_{\mu\nu}/2$. In the Boyer-Linquist coordinates, the effective mass square can be expressed as

$$\mu_{\text{eff}}^2 = -\frac{\alpha Q^2 (r^4 - 6a^2 r^2 \cos^2 \theta + a^4 \cos^4 \theta)}{(r^2 + a^2 \cos^2 \theta)^4}, \quad (3)$$

where Q is the black hole charge, and a represents the ratio of black hole angular momentum J to mass M (i.e., $a \equiv J/M$). Notably, tachyonic instabilities arise in the presence of a negative effective mass square $\mu_{\text{eff}}^2 < 0$, which could induce scalarized black holes from the scalar-free background. When restricted to the equatorial plane, the effective mass square reduces to $\mu_{\text{eff}}^2 = -\alpha Q^2/r^4$, which coincides with the RN black hole case [39, 60]. In the RN black hole background, it has demonstrated that the tachyonic instabilities near the black hole event horizon can be strong enough to trigger spontaneous scalarization. By analogy, we expect similar tachyonic instabilities to induce scalarized KN black holes from the KN black hole background.

To investigate the onset of spontaneous scalarization in KN black holes, we need to solve the linear perturbation equation (2) for zero-modes $\delta\phi(r, \theta)$. The presence of these zero-modes often indicates the existence of scalarized black hole solutions. Specifically, the zero-modes correspond to bifurcation points in the parameter space, marking the onset of scalarized KN black holes. In the latter part of this section, we will discuss the numerical scheme employed to find the zero-modes $\delta\phi(r, \theta)$.

B. Rotating Black Hole Solution

The equations of motion for the metric field $g_{\mu\nu}$, the scalar field ϕ and the electromagnetic field A_μ can be obtained by varying the action (1), yielding

$$\begin{aligned} R_{\mu\nu} - \frac{1}{2}Rg_{\mu\nu} &= 2T_{\mu\nu}, \\ \square\phi - \frac{\alpha}{2}\phi e^{\alpha\phi^2} F^{\mu\nu}F_{\mu\nu} &= 0, \\ \partial_\mu \left(\sqrt{-g} e^{\alpha\phi^2} F^{\mu\nu} \right) &= 0, \end{aligned} \quad (4)$$

where the energy-momentum tensor $T_{\mu\nu}$ is expressed as

$$T_{\mu\nu} = \partial_\mu\phi\partial_\nu\phi - \frac{1}{2}g_{\mu\nu}(\partial\phi)^2 + e^{\alpha\phi^2} \left(F_{\mu\rho}F_\nu{}^\rho - \frac{1}{4}g_{\mu\nu}F_{\rho\sigma}F^{\rho\sigma} \right). \quad (5)$$

Following [37, 77, 78], we consider stationary, axisymmetric and asymptotically-flat black hole solutions with the generic ansatz

$$\begin{aligned} ds^2 &= -e^{2F_0}Ndt^2 + e^{2F_1} \left(\frac{dr^2}{N} + r^2d\theta^2 \right) + e^{2F_2}r^2 \sin^2\theta \left(d\varphi^2 - \frac{W}{r^2}dt \right)^2, \\ A_\mu dx^\mu &= \left(A_t - A_\varphi \frac{W}{r^2} \sin\theta \right) dt + A_\varphi \sin\theta d\varphi \text{ and } \phi = \phi(r, \theta), \end{aligned} \quad (6)$$

where $N \equiv 1 - 1/r_H$, and r_H is the black hole horizon. Here, the metric functions F_0, F_1, F_2, W, A_t and A_φ are assumed to depend solely on the coordinates r and θ . By substituting the ansatz (6) into eqn. (4), we derive a set of nonlinear partial differential equations for the metric functions. The solutions of the partial differential equations can describe scalarized KN black holes with a nontrivial profile of the scalar field or KN black holes with $\phi = 0$.

In the stationary spacetime, two Killing vectors ∂_t and ∂_φ are present, and their combination $\xi = \partial_t + \Omega_H\partial_\varphi$, where Ω_H is the angular velocity of the black hole horizon, is both orthogonal to and null at the horizon. Consequently, the surface gravity κ is defined as $\kappa^2 = -(\nabla_\mu\xi_\nu)(\nabla^\mu\xi^\nu)/2$, and it is related to the Hawking temperature T_H as given in [77]

$$T_H = \frac{\kappa}{2\pi} = \frac{1}{4\pi r_H} e^{F_0(r_H, \theta) - F_1(r_H, \theta)}. \quad (7)$$

In the EMS model, the black hole entropy is expressed as $S = A_H/4$, where the area of the horizon A_H is given by

$$A_H = 2\pi r_H^2 \int_0^\pi d\theta \sin\theta e^{F_1(r_H, \theta) + F_2(r_H, \theta)}. \quad (8)$$

Various physical quantities, such as the black hole mass M , the black hole charge Q , the black hole angular momentum J , the electrostatic potential Φ and the horizon angular velocity Ω_H , can

be determined by studying the asymptotic behavior of the metric functions at the event horizon and spatial infinity [77, 78],

$$\begin{aligned} A_t|_{r=r_H} &\sim 0, & W|_{r=r_H} &\sim r_H^2 \Omega_H, \\ A_t|_{r=\infty} &\sim \Phi - \frac{Q}{r}, & W|_{r=\infty} &\sim \frac{2J}{r}, & e^{2F_0} N|_{r=\infty} &\sim 1 - \frac{2M}{r}. \end{aligned} \quad (9)$$

Moreover, these physical quantities are related by the Smarr relation [60, 77, 79]

$$M = 2T_H S + 2\Omega_H J + \Phi Q, \quad (10)$$

which enables us to assess the accuracy of our numerical black hole solutions.

C. Light Ring

Light rings are null circular geodesics in the black hole spacetime and plays a crucial role in strong gravitational lensing and in the formation of black hole images. For simplicity, we focus on light rings on the equatorial plane. On the equatorial plane, the motion of photons is described by the Lagrangian

$$\mathcal{L} = -\frac{e^{2F_0} N \dot{t}^2}{2} + \frac{e^{2F_1}}{2N} \dot{r}^2 + \frac{e^{2F_2} r^2}{2} \left(\dot{\phi} - \frac{W}{r^2} \dot{t} \right)^2, \quad (11)$$

where dots denote derivatives with respect to an affine parameter λ . The conserved energy E and angular momentum L of photons, associated with the Killing vectors ∂_t and ∂_ϕ , respectively, are expressed as

$$\begin{aligned} E &= \left(e^{2F_0} N - e^{2F_2} \frac{W^2}{r^2} \right) \dot{t} + e^{2F_2} W \dot{\phi}, \\ L &= e^{2F_2} \left(r^2 \dot{\phi} - W \dot{t} \right). \end{aligned} \quad (12)$$

By substituting eqn. (12) into eqn. (11), the constancy of the Lagrangian $\mathcal{L} = 0$ reduces to the radial equation for photons,

$$\dot{r}^2 + V_{\text{eff}} = 0, \quad (13)$$

where $V_{\text{eff}} \leq 0$ for null geodesics. Here, the effective potential is defined as

$$V_{\text{eff}} = L^2 e^{-2F_1} N \left[\frac{e^{-2F_2}}{r^2} - \frac{e^{-2F_0}}{N} \left(\frac{1}{b} - \frac{W}{r^2} \right)^2 \right], \quad (14)$$

where $b \equiv L/E$ is the impact parameter. Thus, for a photon with an impact parameter b_c , it would follow a circular orbit at $r = r_c$ if $V_{\text{eff}}(b_c, r_c) = 0$ and $\partial_r V_{\text{eff}}(b_c, r_c) = 0$.

To facilitate further analysis, we can factorize the effective potential V_{eff} as shown in [80],

$$V_{\text{eff}} = -L^2 e^{-2F_1 - 2F_0} \left(\frac{1}{b} - H_+ \right) \left(\frac{1}{b} - H_- \right), \quad (15)$$

where

$$H_+ = \frac{\sqrt{e^{2F_0 - 2F_2} N r^2 + W}}{r^2}, \quad H_- = -\frac{\sqrt{e^{2F_0 - 2F_2} N r^2 - W}}{r^2}. \quad (16)$$

Notably, the two redefined effective potentials, H_+ and H_- , are independent of the impact parameter and describe prograde and retrograde motion of photons on the equatorial plane, respectively. For a null geodesic, the effective potentials H_+ and H_- must satisfy $H_+ < b^{-1}$ or $H_- > b^{-1}$, where $H_+ \geq H_-$. In particular, a null circular geodesic at $r = r_c$ corresponds to a local extremum of H_+ or H_- , meaning $\partial_r H_+(r_c) = 0$ or $\partial_r H_-(r_c) = 0$. Moreover, $\partial_r^2 H_+(r_c) > 0$ and $\partial_r^2 H_+(r_c) < 0$ indicate stable and unstable prograde light rings, respectively, while $\partial_r^2 H_-(r_c) < 0$ and $\partial_r^2 H_-(r_c) > 0$ correspond to stable and unstable retrograde light rings, respectively. It is worth mentioning that in the static case with $W = 0$, light rings can be solely determined by either H_+ or H_- since $H_+ = -H_-$.

D. Numerical Scheme

In this paper, we utilize pseudospectral methods to numerically solve the linear partial differential equation (2) for zero-modes $\delta\phi(r, \theta)$ and a set of coupled nonlinear partial differential equations for scalarized KN black holes. Pseudospectral methods are a well-established approach for solving partial differential equations [81]. They approximate the exact solution by a finite linear combination of basis functions. Notably, as the number of degrees-of-freedom increases, pseudospectral methods exhibit an exponential convergence rate for well-behaved functions, in contrast to the linear or polynomial convergence of finite difference or finite element methods. Recently, these pseudospectral methods have demonstrated successful applications in searching for black hole solutions [79, 82, 83], as well as computing black hole quasinormal modes [84–86]. For technical details of pseudospectral methods in the context of black hole physics, interested readers can refer to [79].

For the numerical implementation, we introduce a new radial variable given by

$$x = \frac{\sqrt{r^2 - r_H^2} - r_H}{\sqrt{r^2 - r_H^2} + r_H}, \quad (17)$$

which allows us to map the event horizon and spatial infinity to $x = -1$ and $x = 1$, respectively. By performing series expansions of the solutions at the event horizon, we obtain the corresponding

boundary conditions

$$\partial_x \delta\phi = \partial_x F_0 = \partial_x F_1 = \partial_x F_2 = \partial_x \phi = \partial_x A_\varphi = A_t = W - \Omega_H = 0 \text{ at } x = -1. \quad (18)$$

Moreover, due to the flatness at the spatial infinity, we have

$$\delta\phi = F_0 = F_1 = F_2 = \phi = A_\varphi = A_t - \Phi = W = 0 \text{ at } x = 1. \quad (19)$$

On the other hand, the regularity on the symmetric axis imposes the conditions

$$\partial_\theta \delta\phi = \partial_\theta F_0 = \partial_\theta F_1 = \partial_\theta F_2 = \partial_\theta \phi = \partial_\theta A_\varphi = \partial_\theta A_t = \partial_\theta W = 0 \text{ at } \theta = 0 \text{ and } \pi. \quad (20)$$

Since all solutions are symmetric with respect to the equatorial plane, we can restrict the analysis to the upper half domain with $0 \leq \theta \leq \pi/2$, and hence replace the $\theta = \pi$ boundary condition in eqn. (20) with

$$\partial_\theta \delta\phi = \partial_\theta F_0 = \partial_\theta F_1 = \partial_\theta F_2 = \partial_\theta \phi = \partial_\theta A_\varphi = \partial_\theta A_t = \partial_\theta W = 0 \text{ at } \theta = \pi/2. \quad (21)$$

Consequently, eqns. (18), (19), (20) and (21) serve as boundary conditions for solving the partial differential equations. Additionally, the absence of conical singularities requires $F_1 = F_2$ on the symmetric axis, which can be used to verify our numerical results as well as the Smarr relation [37, 77].

With the compactified radial coordinate x , the functions of interest, which are collectively denoted by $\mathcal{F} = \{F_0, F_1, F_2, W, A_t, A_\varphi, \phi, \delta\phi\}$, can be decomposed into a spectral expansion,

$$\mathcal{F}^{(k)} = \sum_{i=0}^{N_x-1} \sum_{j=0}^{N_\theta-1} \alpha_{ij}^{(k)} T_i(x) \cos(2j\theta). \quad (22)$$

Here, N_x and N_θ represent the resolutions in the radial and angular coordinates, respectively, $T_i(x)$ is the Chebyshev polynomial, and $\alpha_{ij}^{(k)}$ are the spectral coefficients. To ensure numerical precision and efficiency, we set $(N_x, N_\theta) = (22, 5)$ and $(N_x, N_\theta) = (42, 8)$ for the subsequent numerical computations of the zero-modes and the metric functions, respectively. To determine $\alpha_{ij}^{(k)}$, we substitute the spectral expansions (22) into the partial differential equations and discretize the resulting equations at the Gauss-Chebyshev points. This process reduces the partial differential equations of \mathcal{F} to a finite system of algebraic equations of α_{ij} . We then solve these algebraic equations for α_{ij} by a standard iterative Newton-Raphson method, where the resulting linear system of equations is solved using the built-in command `LinearSolve` in Mathematica.

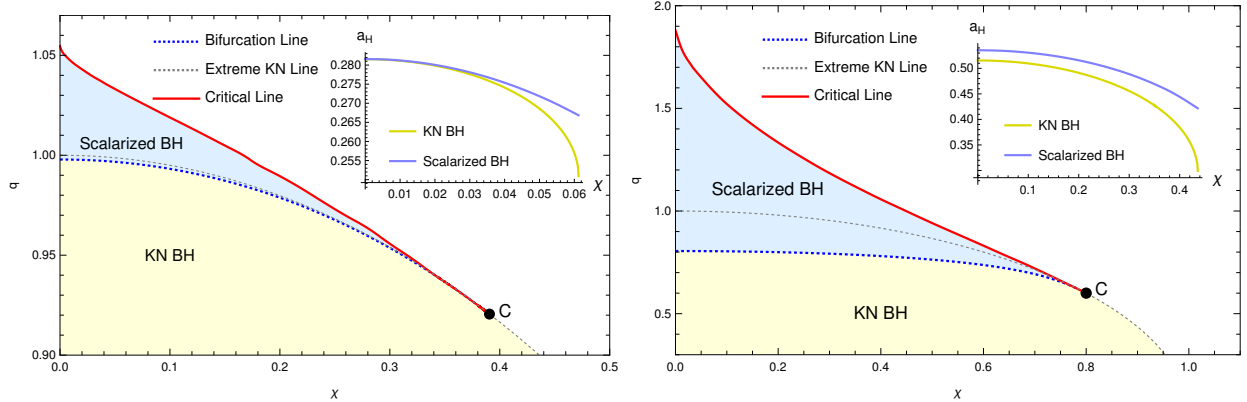


FIG. 1. Domain of existence for scalarized KN black holes in the q - χ plane, with $\alpha = 0.8$ (**left**) and $\alpha = 5$ (**right**), depicted by the regions shaded in light blue. The domain of existence is bounded by the bifurcation and critical lines. The blue dashed lines represent the bifurcation lines, indicating the points where scalarized black holes emerge from KN black holes as zero modes. Meanwhile, the red lines indicate critical configurations of scalarized black holes, characterized by a vanishing horizon area while the mass and charge remain finite. Interestingly, as the black hole spin increases, the bifurcation and critical lines approach each other and eventually converge at the critical point C , illustrating the suppressive effect of rotation on scalarization. KN black holes are situated below the extreme lines, marked by dashed gray lines, and coexist with scalarized black holes in the regions lying between the bifurcation and extreme lines. The insets in the left and right panels depict the reduced horizon area as a function of χ for $q = 0.998$ scalarized black holes with $\alpha = 0.8$ and $q = 0.900$ scalarized black holes with $\alpha = 5$, respectively. These insets demonstrate that scalarized black holes are entropically favored in the coexistence regions.

III. NUMERICAL RESULTS

In this section, we explore the domain of existence for scalarized KN black hole solutions and conduct an analysis of the light ring structure. To facilitate our study, we introduce dimensionless reduced quantities, $q \equiv Q/M$, $\chi \equiv a/M$ and $a_H \equiv A_H/16\pi M^2$. Throughout the numerical implementation, we carefully assess the accuracy of the black hole solutions by verifying the absence of conical singularities and the Smarr relation. Our results reveal that the scalarized KN black hole solutions exhibit a numerical error on the order of 10^{-8} .

A. Domain of Existence

To determine the existence domain of scalarized KN black holes, we adopt a step-by-step approach. Initially, we obtain scalarized black hole solutions along the extreme line of KN black holes by iteratively using the solution from the previous step as the starting values for Newton-Raphson

computations at the current step. This procedure starts with the scalarized RN black hole solution, where $q = 1$, and gradually leads to scalarized KN black hole solutions on the extreme line. Subsequently, we proceed by varying q to compute scalarized black hole solutions along χ -constant lines until it becomes unfeasible to find additional solutions.

In Fig. 1, the left and right panels present the existence domain of scalarized KN black holes with $\alpha = 0.8$ and $\alpha = 5$, respectively, in the q - χ parameter space. The light blue region represents the domain where scalarized black holes exist, and it is delimited by the bifurcation line and the critical line. The bifurcation lines indicate the threshold where the tachyonic instabilities near the event horizon of scalar-free black holes are strong enough to trigger the formation of scalarized black holes. Remarkably, our numerical findings demonstrate that the bifurcation lines coincide perfectly with the zero-mode lines in the q - χ parameter space. This coincidence is expected since scalarized black hole solutions originate from the bifurcation lines as zero modes. On the other hand, scalarized black hole solutions lying on the critical lines possess a vanishing horizon area, while the black hole mass M and charge Q remain finite.

Fig. 1 demonstrates the occurrence of spontaneous scalarization in the EMS model for rotating black holes; however, it is suppressed for high spins. Notably, the bifurcation and critical lines converge and terminate at the critical point C on the extreme line, setting an upper limit on the spin of scalarized black holes. This observation suggests that sufficiently large spin values mitigate tachyonic instabilities, thereby impeding the initiation of spontaneous scalarizations. Moreover, a larger coupling constant α facilitates the scalarization of KN black holes, leading to an expansion of the existence domain for scalarized black holes.

Of particular interest is the coexistence region where scalarized and KN black holes both exist, and this region is delimited by the bifurcation and extreme lines. The inset in each panel displays that scalarized black holes consistently exhibit a greater reduced area of the event horizon when compared to KN black holes. This compelling observation suggests that within the coexistence region, scalarized black holes are entropically favored over scalar-free black holes. Lastly, it is worth noting that scalarized black holes can be overcharged in the parameter region lying between the extremal and critical lines.

B. Light Ring Structure

As discussed earlier, the maxima and minima of H_+ correspond to unstable and stable prograde light rings, respectively, while the maxima and minima of H_- correspond to stable and unstable

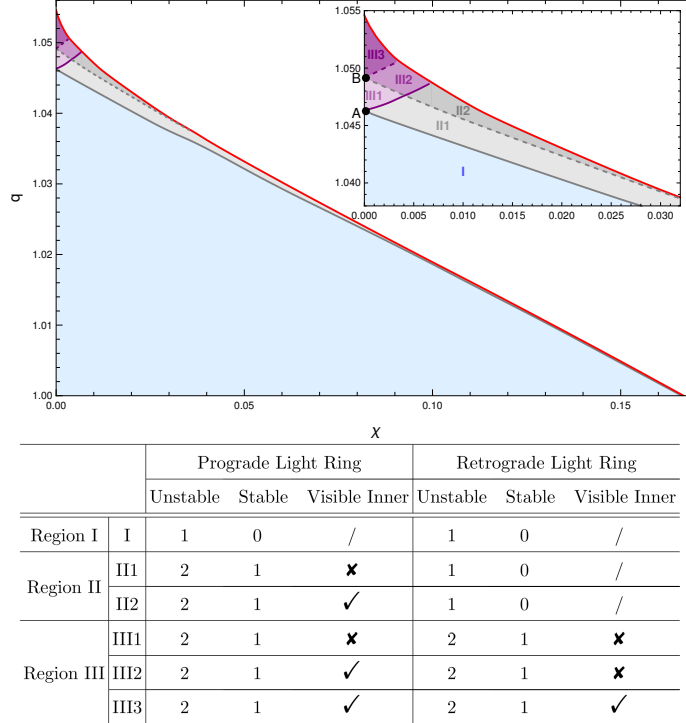


FIG. 2. **Upper:** Scalarized black holes exhibit distinct light ring structures in various regions of the q - χ plane. The boundaries separating these regions are represented by threshold curves, and the corresponding effective potentials are illustrated in FIG. 3. Here, we set $\alpha = 0.8$. **Lower:** The table displays the number of unstable and stable light rings for scalarized black holes in the six regions as shown in the upper panel. The table header “Visible Inner” indicates whether photons originating from inner light rings can reach a distant observer.

retrograde light rings, respectively. To study the light ring structure on the equatorial plane, we investigate the extrema of the effective potentials H_+ and H_- for scalarized KN black holes. In the upper panel of FIG. 2, we present the light ring structure for scalarized black holes with $\alpha = 0.8$ in the q - χ plane, with a zoomed-in inset providing more details. When $\chi = 0$, the threshold points A with $q_A = 1.0463$ and B with $q_B = 1.0492$ determine the structure of light rings (or equivalently, photon spheres in the static case) for scalarized RN black holes. The black lines in the left and right panels of FIG. 3 represent the effective potentials of scalarized RN black holes at points A and B , respectively. At the threshold point A , the effective potential H_+ (H_-) displays a maximum (minimum) and an inflection point, which splits into a minimum (maximum) and an additional maximum (minimum) for $q > q_A$. Consequently, scalarized RN black holes with $q > q_A$ possess two unstable and one stable light rings. On the other hand, at the threshold point B , there are two potential peaks (well) of the effective potential H_+ (H_-) with the same height (depth). For

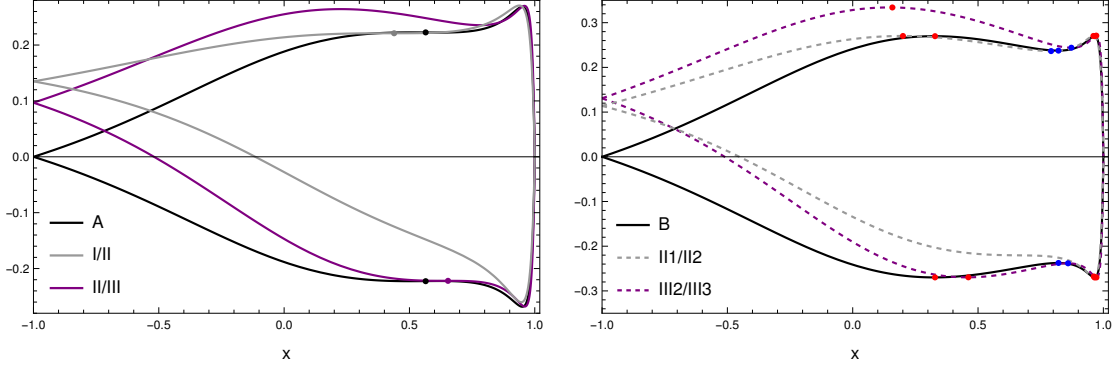


FIG. 3. The effective potentials as a function of x for scalarized black holes with $\alpha = 0.8$ on the threshold curves. The upper and lower branches of the effective potentials denotes the prograde potential H_+ and the retrograde potential H_- , respectively. **Left:** The effective potentials are displayed for the black hole with $q = 1.0463$ and $\chi = 0$ at point A , the one with $q = 1.0400$ and $\chi = 0.0202$ on the I/II curve, and the one with $q = 1.0475$ and $\chi = 0.0038$ on the II/III curve. Inflection points are marked with colored dots, which transform into a maximum and a minimum as q increases. **Right:** The effective potentials are shown for the black hole with $q = 1.0492$ and $\chi = 0$ at point B , the one with $q = 1.0475$ and $\chi = 0.0044$ on the II1/II2 curve, and the one with $q = 1.0500$ and $\chi = 0.0021$ on the III2/III3 curve. Unstable and stable light rings are represented by red and blue dots, respectively. The potential peaks or wells at two unstable light rings possess identical height or depth for H_{\pm} at point B , H_+ on the II1/II2 curve and H_- on the III2/III3 curve.

$q > q_B$, the potential peak (well) at the inner light ring is higher (lower) than the one at the outer ring, indicating that the inner light ring is visible to a distant observer, and thus plays a significant role in determining the optical appearances of luminous matters [65–68]. Accordingly, light rings at the higher (lower) inner potential peak (well) of H_+ (H_-) are referred to as visible inner light rings hereinafter.

As scalarized black holes acquire spin, a single threshold point transforms into two threshold curves, each associated with prograde and retrograde light rings, respectively. In FIG. 2, the resulting four threshold curves are as follows:

- The I/II curve, represented by the solid gray line, exhibits a maximum and an inflection point in H_+ . The left panel of FIG. 3 provides a typical example of the effective potentials, depicted by the solid gray lines.
- The II/III curve, shown by the solid purple line, features a minimum and an inflection point in H_- . The left panel of FIG. 3 illustrates a typical example of the effective potentials, denoted by the solid purple lines.

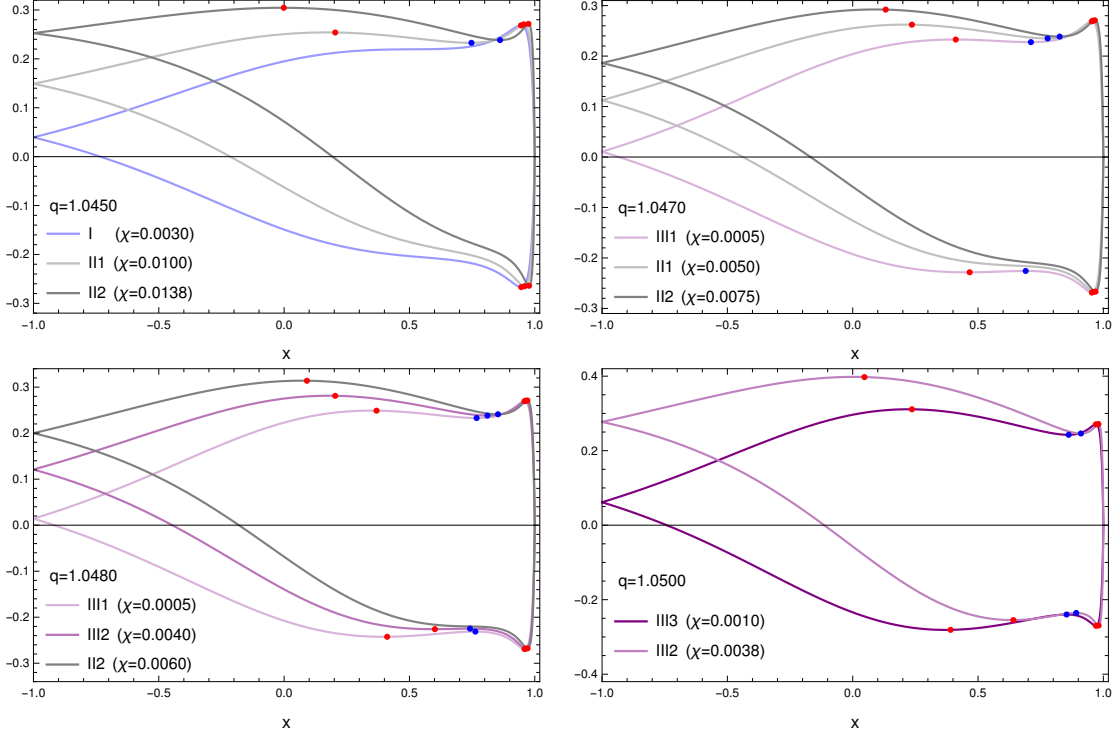


FIG. 4. The effective potentials as a function of x for representative scalarized black hole solutions with $\alpha = 0.8$ in the regions characterized by distinct light ring structures. The upper and lower branches of the effective potentials are denoted as the prograde potential H_+ and the retrograde potential H_- , respectively. Red and blue dots represent unstable and stable light rings, respectively.

- The II1/II2 curve, denoted by the dashed gray line, has two potential peaks of H_+ at the same height. The right panel of FIG. 3 displays a typical example of the effective potentials, represented by the dashed grays.
- The III2/III3 curve, indicated by the dashed purple line, involves two potential wells of H_- with the same depth. The right panel of FIG. 3 shows a typical example of the effective potentials, depicted by the dashed purple lines.

As a consequence, the four threshold curves partition the domain of existence into six regions, each corresponding to a distinct light ring structure, as depicted in the upper panel of FIG. 2. The light ring properties in these six regions are presented in the lower table of FIG. 2. Additionally, we showcase the effective potentials of representative black hole solutions in FIG. 4. Remarkably, our findings indicate that the number of unstable light rings is always one greater than the number of stable ones, consistent with prior observations in [87]. Intriguingly, for a given q , a sufficiently high spin can engender multiple light rings, even from scalarized RN black holes with only one

light ring. Lastly, it is worth noting that prograde photons are more likely to possess multiple light rings compared to retrograde photons.

IV. CONCLUSIONS

This paper first presented our numerical construction of scalarized rotating black hole solutions within the EMS model and explored the parameter regions in which these solutions exist. The EMS model incorporates a non-minimal coupling between the scalar and electromagnetic fields, leading to tachyonic instabilities that can trigger the formation of scalarized KN black holes. Our findings demonstrated that the black hole spin tends to inhibit the spontaneous scalarization of KN black holes, and scalarized KN black holes cease to exist beyond a certain threshold spin. Later, we delved into the light ring structure of scalarized KN black holes. We found that slowly-rotating scalarized black holes with a small electric charge typically possess one unstable prograde and one unstable retrograde light rings. However, as scalarized black holes spin faster, two unstable and one stable prograde light rings can emerge. Additionally, for sufficiently large black hole charge, two unstable and one stable retrograde light rings can also be observed.

While our focus has been on positive coupling constants α , it is noteworthy that studies involving negative coupling constants α have revealed tachyonic instabilities leading to unstable perturbations for large black hole spin [88, 89]. Investigating the existence of scalarized black holes with negative coupling constants α and understanding their formation from scalar-free black holes are promising avenues for future research. Furthermore, this work has shed light on the intricate behavior of scalarized rotating black holes within the EMS model. Future studies may explore the stability of these solutions and investigate their observable signatures, taking advantage of the rich light ring structure they exhibit. Such investigations will further enhance our understanding of rotating black holes with multiple light rings and contribute to the broader field of black hole physics.

ACKNOWLEDGMENTS

We are grateful to Yiqian Chen and Qingyu Gan for useful discussions and valuable comments. This work is supported in part by NSFC (Grant No. 12105191, 11947225 and 11875196). Houwen Wu is supported by the International Visiting Program for Excellent Young Scholars of Sichuan

University.

- [1] B.P. Abbott et al. Observation of Gravitational Waves from a Binary Black Hole Merger. *Phys. Rev. Lett.*, 116(6):061102, 2016. [arXiv:1602.03837](#), [doi:10.1103/PhysRevLett.116.061102](#). I
- [2] Emanuele Berti, Vitor Cardoso, Jose A. Gonzalez, and Ulrich Sperhake. Mining information from binary black hole mergers: A Comparison of estimation methods for complex exponentials in noise. *Phys. Rev. D*, 75:124017, 2007. [arXiv:gr-qc/0701086](#), [doi:10.1103/PhysRevD.75.124017](#). I
- [3] Richard H. Price and Gaurav Khanna. Gravitational wave sources: reflections and echoes. *Class. Quant. Grav.*, 34(22):225005, 2017. [arXiv:1702.04833](#), [doi:10.1088/1361-6382/aa8f29](#). I
- [4] Matthew Giesler, Maximiliano Isi, Mark A. Scheel, and Saul Teukolsky. Black Hole Ringdown: The Importance of Overtones. *Phys. Rev. X*, 9(4):041060, 2019. [arXiv:1903.08284](#), [doi:10.1103/PhysRevX.9.041060](#). I
- [5] Kazunori Akiyama et al. First M87 Event Horizon Telescope Results. IV. Imaging the Central Supermassive Black Hole. *Astrophys. J. Lett.*, 875(1):L4, 2019. [arXiv:1906.11241](#), [doi:10.3847/2041-8213/ab0e85](#). I
- [6] Kazunori Akiyama et al. First M87 Event Horizon Telescope Results. II. Array and Instrumentation. *Astrophys. J. Lett.*, 875(1):L2, 2019. [arXiv:1906.11239](#), [doi:10.3847/2041-8213/ab0c96](#).
- [7] Kazunori Akiyama et al. First M87 Event Horizon Telescope Results. I. The Shadow of the Supermassive Black Hole. *Astrophys. J. Lett.*, 875:L1, 2019. [arXiv:1906.11238](#), [doi:10.3847/2041-8213/ab0ec7](#).
- [8] Kazunori Akiyama et al. First M87 Event Horizon Telescope Results. VI. The Shadow and Mass of the Central Black Hole. *Astrophys. J. Lett.*, 875(1):L6, 2019. [arXiv:1906.11243](#), [doi:10.3847/2041-8213/ab1141](#).
- [9] Kazunori Akiyama et al. First M87 Event Horizon Telescope Results. V. Physical Origin of the Asymmetric Ring. *Astrophys. J. Lett.*, 875(1):L5, 2019. [arXiv:1906.11242](#), [doi:10.3847/2041-8213/ab0f43](#).
- [10] Kazunori Akiyama et al. First M87 Event Horizon Telescope Results. III. Data Processing and Calibration. *Astrophys. J. Lett.*, 875(1):L3, 2019. [arXiv:1906.11240](#), [doi:10.3847/2041-8213/ab0c57](#).
- [11] Kazunori Akiyama et al. First Sagittarius A* Event Horizon Telescope Results. IV. Variability, Morphology, and Black Hole Mass. *Astrophys. J. Lett.*, 930(2):L15, 2022. [doi:10.3847/2041-8213/ac6736](#).
- [12] Kazunori Akiyama et al. First Sagittarius A* Event Horizon Telescope Results. V. Testing Astrophysical Models of the Galactic Center Black Hole. *Astrophys. J. Lett.*, 930(2):L16, 2022. [doi:10.3847/2041-8213/ac6672](#).
- [13] Kazunori Akiyama et al. First Sagittarius A* Event Horizon Telescope Results. II. EHT and Multiwavelength Observations, Data Processing, and Calibration. *Astrophys. J. Lett.*, 930(2):L13, 2022.

- [doi:10.3847/2041-8213/ac6675](https://doi.org/10.3847/2041-8213/ac6675).
- [14] Kazunori Akiyama et al. First Sagittarius A* Event Horizon Telescope Results. III. Imaging of the Galactic Center Supermassive Black Hole. *Astrophys. J. Lett.*, 930(2):L14, 2022. [doi:10.3847/2041-8213/ac6429](https://doi.org/10.3847/2041-8213/ac6429).
- [15] Kazunori Akiyama et al. First Sagittarius A* Event Horizon Telescope Results. I. The Shadow of the Supermassive Black Hole in the Center of the Milky Way. *Astrophys. J. Lett.*, 930(2):L12, 2022. [doi:10.3847/2041-8213/ac6674](https://doi.org/10.3847/2041-8213/ac6674).
- [16] Kazunori Akiyama et al. First Sagittarius A* Event Horizon Telescope Results. VI. Testing the Black Hole Metric. *Astrophys. J. Lett.*, 930(2):L17, 2022. [doi:10.3847/2041-8213/ac6756](https://doi.org/10.3847/2041-8213/ac6756). I
- [17] Werner Israel. Event horizons in static vacuum space-times. *Phys. Rev.*, 164:1776–1779, 1967. [doi:10.1103/PhysRev.164.1776](https://doi.org/10.1103/PhysRev.164.1776). I
- [18] B. Carter. Axisymmetric Black Hole Has Only Two Degrees of Freedom. *Phys. Rev. Lett.*, 26:331–333, 1971. [doi:10.1103/PhysRevLett.26.331](https://doi.org/10.1103/PhysRevLett.26.331).
- [19] Remo Ruffini and John A. Wheeler. Introducing the black hole. *Phys. Today*, 24(1):30, 1971. [doi:10.1063/1.3022513](https://doi.org/10.1063/1.3022513). I
- [20] M.S. Volkov and D.V. Galtsov. NonAbelian Einstein Yang-Mills black holes. *JETP Lett.*, 50:346–350, 1989. I
- [21] P. Bizon. Colored black holes. *Phys. Rev. Lett.*, 64:2844–2847, 1990. [doi:10.1103/PhysRevLett.64.2844](https://doi.org/10.1103/PhysRevLett.64.2844).
- [22] Brian R. Greene, Samir D. Mathur, and Christopher M. O’Neill. Eluding the no hair conjecture: Black holes in spontaneously broken gauge theories. *Phys. Rev. D*, 47:2242–2259, 1993. [arXiv:hep-th/9211007](https://arxiv.org/abs/hep-th/9211007), [doi:10.1103/PhysRevD.47.2242](https://doi.org/10.1103/PhysRevD.47.2242).
- [23] Hugh Luckock and Ian Moss. BLACK HOLES HAVE SKYRMION HAIR. *Phys. Lett. B*, 176:341–345, 1986. [doi:10.1016/0370-2693\(86\)90175-9](https://doi.org/10.1016/0370-2693(86)90175-9).
- [24] Serge Droz, Markus Heusler, and Norbert Straumann. New black hole solutions with hair. *Phys. Lett. B*, 268:371–376, 1991. [doi:10.1016/0370-2693\(91\)91592-J](https://doi.org/10.1016/0370-2693(91)91592-J).
- [25] P. Kanti, N.E. Mavromatos, J. Rizos, K. Tamvakis, and E. Winstanley. Dilatonic black holes in higher curvature string gravity. *Phys. Rev. D*, 54:5049–5058, 1996. [arXiv:hep-th/9511071](https://arxiv.org/abs/hep-th/9511071), [doi:10.1103/PhysRevD.54.5049](https://doi.org/10.1103/PhysRevD.54.5049).
- [26] Subhash Mahapatra, Supragyan Priyadarshinee, Gosala Narasimha Reddy, and Bhaskar Shukla. Exact topological charged hairy black holes in AdS Space in D -dimensions. *Phys. Rev. D*, 102(2):024042, 2020. [arXiv:2004.00921](https://arxiv.org/abs/2004.00921), [doi:10.1103/PhysRevD.102.024042](https://doi.org/10.1103/PhysRevD.102.024042). I
- [27] Thibault Damour and Gilles Esposito-Farese. Nonperturbative strong field effects in tensor - scalar theories of gravitation. *Phys. Rev. Lett.*, 70:2220–2223, 1993. [doi:10.1103/PhysRevLett.70.2220](https://doi.org/10.1103/PhysRevLett.70.2220). I
- [28] Ivan Zh. Stefanov, Stoytcho S. Yazadjiev, and Michail D. Todorov. Phases of 4D scalar-tensor black holes coupled to Born-Infeld nonlinear electrodynamics. *Mod. Phys. Lett. A*, 23:2915–2931, 2008. [arXiv:0708.4141](https://arxiv.org/abs/0708.4141), [doi:10.1142/S0217732308028351](https://doi.org/10.1142/S0217732308028351). I

- [29] Daniela D. Doneva, Stoytcho S. Yazadjiev, Kostas D. Kokkotas, and Ivan Zh. Stefanov. Quasi-normal modes, bifurcations and non-uniqueness of charged scalar-tensor black holes. *Phys. Rev. D*, 82:064030, 2010. [arXiv:1007.1767](#), [doi:10.1103/PhysRevD.82.064030](#). I
- [30] Vitor Cardoso, Isabella P. Carucci, Paolo Pani, and Thomas P. Sotiriou. Matter around Kerr black holes in scalar-tensor theories: scalarization and superradiant instability. *Phys. Rev. D*, 88:044056, 2013. [arXiv:1305.6936](#), [doi:10.1103/PhysRevD.88.044056](#). I
- [31] Vitor Cardoso, Isabella P. Carucci, Paolo Pani, and Thomas P. Sotiriou. Black holes with surrounding matter in scalar-tensor theories. *Phys. Rev. Lett.*, 111:111101, 2013. [arXiv:1308.6587](#), [doi:10.1103/PhysRevLett.111.111101](#). I
- [32] Daniela D. Doneva and Stoytcho S. Yazadjiev. New Gauss-Bonnet Black Holes with Curvature-Induced Scalarization in Extended Scalar-Tensor Theories. *Phys. Rev. Lett.*, 120(13):131103, 2018. [arXiv:1711.01187](#), [doi:10.1103/PhysRevLett.120.131103](#). I
- [33] Hector O. Silva, Jeremy Sakstein, Leonardo Gualtieri, Thomas P. Sotiriou, and Emanuele Berti. Spontaneous scalarization of black holes and compact stars from a Gauss-Bonnet coupling. *Phys. Rev. Lett.*, 120(13):131104, 2018. [arXiv:1711.02080](#), [doi:10.1103/PhysRevLett.120.131104](#).
- [34] G. Antoniou, A. Bakopoulos, and P. Kanti. Evasion of No-Hair Theorems and Novel Black-Hole Solutions in Gauss-Bonnet Theories. *Phys. Rev. Lett.*, 120(13):131102, 2018. [arXiv:1711.03390](#), [doi:10.1103/PhysRevLett.120.131102](#).
- [35] Daniela D. Doneva, Stella Kiorpelidi, Petya G. Nedkova, Eleftherios Papantonopoulos, and Stoytcho S. Yazadjiev. Charged Gauss-Bonnet black holes with curvature induced scalarization in the extended scalar-tensor theories. *Phys. Rev. D*, 98(10):104056, 2018. [arXiv:1809.00844](#), [doi:10.1103/PhysRevD.98.104056](#).
- [36] Pedro V.P. Cunha, Carlos A.R. Herdeiro, and Eugen Radu. Spontaneously Scalarized Kerr Black Holes in Extended Scalar-Tensor–Gauss-Bonnet Gravity. *Phys. Rev. Lett.*, 123(1):011101, 2019. [arXiv:1904.09997](#), [doi:10.1103/PhysRevLett.123.011101](#). I
- [37] Carlos A. R. Herdeiro, Eugen Radu, Hector O. Silva, Thomas P. Sotiriou, and Nicolás Yunes. Spin-induced scalarized black holes. *Phys. Rev. Lett.*, 126(1):011103, 2021. [arXiv:2009.03904](#), [doi:10.1103/PhysRevLett.126.011103](#). I, II B, II D
- [38] Emanuele Berti, Lucas G. Collodel, Burkhard Kleihaus, and Jutta Kunz. Spin-induced black-hole scalarization in Einstein-scalar-Gauss-Bonnet theory. *Phys. Rev. Lett.*, 126(1):011104, 2021. [arXiv:2009.03905](#), [doi:10.1103/PhysRevLett.126.011104](#). I
- [39] Carlos A.R. Herdeiro, Eugen Radu, Nicolas Sanchis-Gual, and José A. Font. Spontaneous Scalarization of Charged Black Holes. *Phys. Rev. Lett.*, 121(10):101102, 2018. [arXiv:1806.05190](#), [doi:10.1103/PhysRevLett.121.101102](#). I, II, II A
- [40] Pedro G. S. Fernandes, Carlos A. R. Herdeiro, Alexandre M. Pombo, Eugen Radu, and Nicolas Sanchis-Gual. Spontaneous Scalarisation of Charged Black Holes: Coupling Dependence and Dynamical Features. *Class. Quant. Grav.*, 36(13):134002, 2019. [Erratum: *Class.Quant.Grav.* 37, 049501 (2020)].

- [arXiv:1902.05079](#), [doi:10.1088/1361-6382/ab23a1](#). I, II
- [41] Pedro G.S. Fernandes, Carlos A.R. Herdeiro, Alexandre M. Pombo, Eugen Radu, and Nicolas Sanchis-Gual. Charged black holes with axionic-type couplings: Classes of solutions and dynamical scalarization. *Phys. Rev. D*, 100(8):084045, 2019. [arXiv:1908.00037](#), [doi:10.1103/PhysRevD.100.084045](#).
- [42] Jose Luis Blázquez-Salcedo, Carlos A.R. Herdeiro, Jutta Kunz, Alexandre M. Pombo, and Eugen Radu. Einstein-Maxwell-scalar black holes: the hot, the cold and the bald. *Phys. Lett. B*, 806:135493, 2020. [arXiv:2002.00963](#), [doi:10.1016/j.physletb.2020.135493](#). I
- [43] De-Cheng Zou and Yun Soo Myung. Scalarized charged black holes with scalar mass term. *Phys. Rev. D*, 100(12):124055, 2019. [arXiv:1909.11859](#), [doi:10.1103/PhysRevD.100.124055](#). I
- [44] Pedro G.S. Fernandes. Einstein-Maxwell-scalar black holes with massive and self-interacting scalar hair. *Phys. Dark Univ.*, 30:100716, 2020. [arXiv:2003.01045](#), [doi:10.1016/j.dark.2020.100716](#). I
- [45] Yan Peng. Scalarization of horizonless reflecting stars: neutral scalar fields non-minimally coupled to Maxwell fields. *Phys. Lett. B*, 804:135372, 2020. [arXiv:1912.11989](#), [doi:10.1016/j.physletb.2020.135372](#). I
- [46] Yun Soo Myung and De-Cheng Zou. Instability of Reissner–Nordström black hole in Einstein–Maxwell-scalar theory. *Eur. Phys. J. C*, 79(3):273, 2019. [arXiv:1808.02609](#), [doi:10.1140/epjc/s10052-019-6792-6](#). I
- [47] Yun Soo Myung and De-Cheng Zou. Stability of scalarized charged black holes in the Einstein–Maxwell–Scalar theory. *Eur. Phys. J. C*, 79(8):641, 2019. [arXiv:1904.09864](#), [doi:10.1140/epjc/s10052-019-7176-7](#).
- [48] De-Cheng Zou and Yun Soo Myung. Radial perturbations of the scalarized black holes in Einstein–Maxwell-conformally coupled scalar theory. *Phys. Rev. D*, 102(6):064011, 2020. [arXiv:2005.06677](#), [doi:10.1103/PhysRevD.102.064011](#).
- [49] Yun Soo Myung and De-Cheng Zou. Onset of rotating scalarized black holes in Einstein–Chern–Simons–Scalar theory. *Phys. Lett. B*, 814:136081, 2021. [arXiv:2012.02375](#), [doi:10.1016/j.physletb.2021.136081](#).
- [50] Zhan-Feng Mai and Run-Qiu Yang. Stability analysis of a charged black hole with a nonlinear complex scalar field. *Phys. Rev. D*, 104(4):044008, 2021. [arXiv:2101.00026](#), [doi:10.1103/PhysRevD.104.044008](#). I
- [51] Dumitru Astefanesei, Carlos Herdeiro, João Oliveira, and Eugen Radu. Higher dimensional black hole scalarization. *JHEP*, 09:186, 2020. [arXiv:2007.04153](#), [doi:10.1007/JHEP09\(2020\)186](#). I
- [52] Yun Soo Myung and De-Cheng Zou. Quasinormal modes of scalarized black holes in the Einstein–Maxwell–Scalar theory. *Phys. Lett. B*, 790:400–407, 2019. [arXiv:1812.03604](#), [doi:10.1016/j.physletb.2019.01.046](#). I
- [53] Jose Luis Blázquez-Salcedo, Carlos A.R. Herdeiro, Sarah Kahlen, Jutta Kunz, Alexandre M. Pombo, and Eugen Radu. Quasinormal modes of hot, cold and bald Einstein–Maxwell-scalar black holes. 8 2020. [arXiv:2008.11744](#). I

- [54] Yun Soo Myung and De-Cheng Zou. Scalarized charged black holes in the Einstein-Maxwell-Scalar theory with two U(1) fields. *Phys. Lett. B*, 811:135905, 2020. [arXiv:2009.05193](#), [doi:10.1016/j.physletb.2020.135905](#). I
- [55] Yun Soo Myung and De-Cheng Zou. Scalarized black holes in the Einstein-Maxwell-scalar theory with a quasitopological term. *Phys. Rev. D*, 103(2):024010, 2021. [arXiv:2011.09665](#), [doi:10.1103/PhysRevD.103.024010](#). I
- [56] Hong Guo, Xiao-Mei Kuang, Eleftherios Papantonopoulos, and Bin Wang. Topology and spacetime structure influences on black hole scalarization. 12 2020. [arXiv:2012.11844](#). I
- [57] Yves Brihaye, Betti Hartmann, Nathália Pio Aprile, and Jon Urrestilla. Scalarization of asymptotically anti-de Sitter black holes with applications to holographic phase transitions. *Phys. Rev. D*, 101(12):124016, 2020. [arXiv:1911.01950](#), [doi:10.1103/PhysRevD.101.124016](#). I
- [58] Yves Brihaye, Carlos Herdeiro, and Eugen Radu. Black Hole Spontaneous Scalarisation with a Positive Cosmological Constant. *Phys. Lett. B*, 802:135269, 2020. [arXiv:1910.05286](#), [doi:10.1016/j.physletb.2020.135269](#).
- [59] Cheng-Yong Zhang, Peng Liu, Yunqi Liu, Chao Niu, and Bin Wang. Dynamical charged black hole spontaneous scalarization in anti-de Sitter spacetimes. *Phys. Rev. D*, 104(8):084089, 2021. [arXiv:2103.13599](#), [doi:10.1103/PhysRevD.104.084089](#).
- [60] Guangzhou Guo, Peng Wang, Houwen Wu, and Haitang Yang. Scalarized Einstein-Maxwell-scalar black holes in anti-de Sitter spacetime. *Eur. Phys. J. C*, 81(10):864, 2021. [arXiv:2102.04015](#), [doi:10.1140/epjc/s10052-021-09614-7](#). IIA, IIB
- [61] Qian Chen, Zhuan Ning, Yu Tian, Bin Wang, and Cheng-Yong Zhang. Nonlinear dynamics of hot, cold and bald Einstein-Maxwell-scalar black holes in AdS spacetime. 7 2023. [arXiv:2307.03060](#). I
- [62] Cheng-Yong Zhang, Qian Chen, Yunqi Liu, Wen-Kun Luo, Yu Tian, and Bin Wang. Critical Phenomena in Dynamical Scalarization of Charged Black Holes. *Phys. Rev. Lett.*, 128(16):161105, 2022. [arXiv:2112.07455](#), [doi:10.1103/PhysRevLett.128.161105](#). I
- [63] Cheng-Yong Zhang, Qian Chen, Yunqi Liu, Wen-Kun Luo, Yu Tian, and Bin Wang. Dynamical transitions in scalarization and descalarization through black hole accretion. *Phys. Rev. D*, 106(6):L061501, 2022. [arXiv:2204.09260](#), [doi:10.1103/PhysRevD.106.L061501](#).
- [64] Jia-Yan Jiang, Qian Chen, Yunqi Liu, Yu Tian, Wei Xiong, Cheng-Yong Zhang, and Bin Wang. Type I critical dynamical scalarization and descalarization in Einstein-Maxwell-scalar theory. 6 2023. [arXiv:2306.10371](#). I
- [65] Qingyu Gan, Peng Wang, Houwen Wu, and Haitang Yang. Photon spheres and spherical accretion image of a hairy black hole. *Phys. Rev. D*, 104(2):024003, 2021. [arXiv:2104.08703](#), [doi:10.1103/PhysRevD.104.024003](#). I, IIIB
- [66] Qingyu Gan, Peng Wang, Houwen Wu, and Haitang Yang. Photon ring and observational appearance of a hairy black hole. *Phys. Rev. D*, 104(4):044049, 2021. [arXiv:2105.11770](#), [doi:10.1103/PhysRevD.104.044049](#). I

- [67] Guangzhou Guo, Xin Jiang, Peng Wang, and Houwen Wu. Gravitational lensing by black holes with multiple photon spheres. *Phys. Rev. D*, 105(12):124064, 2022. [arXiv:2204.13948](#), [doi:10.1103/PhysRevD.105.124064](#). I
- [68] Yiqian Chen, Guangzhou Guo, Peng Wang, Houwen Wu, and Haitang Yang. Appearance of an infalling star in black holes with multiple photon spheres. *Sci. China Phys. Mech. Astron.*, 65(12):120412, 2022. [arXiv:2206.13705](#), [doi:10.1007/s11433-022-1986-x](#). I, IIIB
- [69] Vitor Cardoso, Luís C. B. Crispino, Caio F. B. Macedo, Hirotada Okawa, and Paolo Pani. Light rings as observational evidence for event horizons: long-lived modes, ergoregions and nonlinear instabilities of ultracompact objects. *Phys. Rev. D*, 90(4):044069, 2014. [arXiv:1406.5510](#), [doi:10.1103/PhysRevD.90.044069](#). I
- [70] Joe Keir. Slowly decaying waves on spherically symmetric spacetimes and ultracompact neutron stars. *Class. Quant. Grav.*, 33(13):135009, 2016. [arXiv:1404.7036](#), [doi:10.1088/0264-9381/33/13/135009](#).
- [71] Minyong Guo, Zhen Zhong, Jinguang Wang, and Sijie Gao. Light rings and long-lived modes in quasiblack hole spacetimes. *Phys. Rev. D*, 105(2):024049, 2022. [arXiv:2108.08967](#), [doi:10.1103/PhysRevD.105.024049](#).
- [72] Guangzhou Guo, Peng Wang, Houwen Wu, and Haitang Yang. Quasinormal modes of black holes with multiple photon spheres. *JHEP*, 06:060, 2022. [arXiv:2112.14133](#), [doi:10.1007/JHEP06\(2022\)060](#).
- [73] Guangzhou Guo, Peng Wang, Houwen Wu, and Haitang Yang. Echoes from hairy black holes. *JHEP*, 06:073, 2022. [arXiv:2204.00982](#), [doi:10.1007/JHEP06\(2022\)073](#). I
- [74] Guangzhou Guo, Peng Wang, Houwen Wu, and Haitang Yang. Superradiance instabilities of charged black holes in Einstein-Maxwell-scalar theory. *JHEP*, 07:070, 2023. [arXiv:2301.06483](#), [doi:10.1007/JHEP07\(2023\)070](#). I
- [75] Guangzhou Guo, Yuhang Lu, Peng Wang, Houwen Wu, and Haitang Yang. Black holes with multiple photon spheres. *Phys. Rev. D*, 107(12):124037, 2023. [arXiv:2212.12901](#), [doi:10.1103/PhysRevD.107.124037](#). I
- [76] Meng-Yun Lai, Yun Soo Myung, Rui-Hong Yue, and De-Cheng Zou. Spin-charge induced spontaneous scalarization of Kerr-Newman black holes. *Phys. Rev. D*, 106(8):084043, 2022. [arXiv:2208.11849](#), [doi:10.1103/PhysRevD.106.084043](#). I
- [77] Carlos Herdeiro and Eugen Radu. Construction and physical properties of Kerr black holes with scalar hair. *Class. Quant. Grav.*, 32(14):144001, 2015. [arXiv:1501.04319](#), [doi:10.1088/0264-9381/32/14/144001](#). IIB, IIB, IIB, IIB, IID
- [78] Jorge F. M. Delgado, Carlos A. R. Herdeiro, Eugen Radu, and Helgi Runarsson. Kerr-Newman black holes with scalar hair. *Phys. Lett. B*, 761:234–241, 2016. [arXiv:1608.00631](#), [doi:10.1016/j.physletb.2016.08.032](#). IIB, IIB
- [79] Pedro G. S. Fernandes and David J. Mulryne. A new approach and code for spinning black holes in modified gravity. *Class. Quant. Grav.*, 40(16):165001, 2023. [arXiv:2212.07293](#), [doi:10.1088/](#)

- [1361-6382/ace232](#). IIB, IID, IID
- [80] P. V. P. Cunha, J. Grover, C. Herdeiro, E. Radu, H. Runarsson, and A. Wittig. Chaotic lensing around boson stars and Kerr black holes with scalar hair. *Phys. Rev. D*, 94(10):104023, 2016. [arXiv:1609.01340](#), [doi:10.1103/PhysRevD.94.104023](#). IIC
- [81] John P Boyd. *Chebyshev and Fourier spectral methods*. Courier Corporation, 2001. IID
- [82] Meng-Yun Lai, De-Cheng Zou, Rui-Hong Yue, and Yun Soo Myung. Nonlinearly scalarized rotating black holes in Einstein-scalar-Gauss-Bonnet theory. 4 2023. [arXiv:2304.08012](#). IID
- [83] Clare Burrage, Pedro G. S. Fernandes, Richard Brito, and Vitor Cardoso. Spinning Black Holes with Axion Hair. 6 2023. [arXiv:2306.03662](#). IID
- [84] Aron Jansen. Overdamped modes in Schwarzschild-de Sitter and a Mathematica package for the numerical computation of quasinormal modes. *Eur. Phys. J. Plus*, 132(12):546, 2017. [arXiv:1709.09178](#), [doi:10.1140/epjp/i2017-11825-9](#). IID
- [85] Qingyu Gan, Guangzhou Guo, Peng Wang, and Houwen Wu. Strong cosmic censorship for a scalar field in a Born-Infeld–de Sitter black hole. *Phys. Rev. D*, 100(12):124009, 2019. [arXiv:1907.04466](#), [doi:10.1103/PhysRevD.100.124009](#).
- [86] Adrian Ka-Wai Chung, Pratik Wagle, and Nicolas Yunes. Spectral method for the gravitational perturbations of black holes: Schwarzschild background case. *Phys. Rev. D*, 107(12):124032, 2023. [arXiv:2302.11624](#), [doi:10.1103/PhysRevD.107.124032](#). IID
- [87] Pedro V. P. Cunha and Carlos A. R. Herdeiro. Stationary black holes and light rings. *Phys. Rev. Lett.*, 124(18):181101, 2020. [arXiv:2003.06445](#), [doi:10.1103/PhysRevLett.124.181101](#). IIIB
- [88] Meng-Yun Lai, Yun Soo Myung, Rui-Hong Yue, and De-Cheng Zou. Spin-induced scalarization of Kerr-Newman black holes in Einstein-Maxwell-scalar theory. *Phys. Rev. D*, 106(4):044045, 2022. [arXiv:2206.11587](#), [doi:10.1103/PhysRevD.106.044045](#). IV
- [89] Shahar Hod. Spin-charge induced scalarization of Kerr-Newman black-hole spacetimes. *JHEP*, 08:272, 2022. [arXiv:2206.12074](#), [doi:10.1007/JHEP08\(2022\)272](#). IV